analytical chemistry

Article

pubs.acs.org/ac

# Ultrasound-Enhanced Attenuated Total Reflection Mid-infrared Spectroscopy In-Line Probe: Acquisition of Cell Spectra in a Bioreactor

Cosima Koch,[†] Markus Brandstetter,[†,§] Patrick Wechselberger,[‡,⊥] Bettina Lorantfy,[‡,∥] Maria Reyes Plata,[†] Stefan Radel,[†] Christoph Herwig,[‡,⊥] and Bernhard Lendl*[,†]

[†]Institute of Chemical Technologies and Analytics, Vienna University of Technology, Getreidemarkt 9/164-UPA, 1060 Vienna, Austria

[‡]Institute of Chemical Engineering, Vienna University of Technology, Gumpendorferstraße 1a, 1060 Vienna, Austria

[⊥]Christian Doppler Laboratory for Mechanistic and Physiological Methods for Improved Bioprocesses, Institute of Chemical Engineering, Vienna University of Technology, Getreidemarkt 9/166, 1060 Vienna, Austria

Supporting Information

**ABSTRACT:** This article presents a novel method for selective acquisition of Fourier transform infrared (FT-IR) spectra of microorganisms in-line during fermentation, using *Saccharomyces cerevisiae* as an example. The position of the cells relative to the sensitive region of the attenuated total reflection (ATR) FT-IR probe was controlled by combing a commercially available ATR in-line probe with contact-free, gentle particle manipulation by ultrasonic standing waves. A prototype probe was successfully constructed, assembled, and tested in-line during fed-batch fermentations of *S. cerevisiae*. Control over the position of the cells was achieved by tuning the ultrasound frequency: 2.41 MHz was used for acquisition of spectra of the cells (pushing frequency $f_p$) and 1.87 MHz, for retracting the cells from the ATR element, therefore allowing spectra of the medium to be acquired. Accumulation of storage carbohydrates (trehalose and glycogen) inside the cells was induced by a lack of a nitrogen source in the feed medium. These changes in biochemical composition were visible in the spectra of the cells recorded in-line during the application of $f_p$ and could be verified by reference spectra of dried cell samples recorded off-line with a FT-IR microscope. Comparison of the cell spectra with spectra of trehalose, glycogen, glucose, and mannan, i.e., the major carbohydrates present in *S. cerevisiae*, and principal components analysis revealed that the changes observed in the cell spectra correlated well with the bands specific for trehalose and glycogen. This proves the applicability and capability of ultrasound-enhanced in-line ATR mid-IR spectroscopy as a real-time PAT method for the in situ monitoring of cellular biochemistry during fermentation.

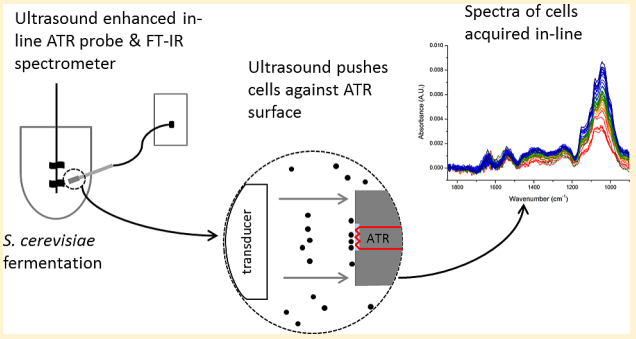


Fourier transform infrared (FT-IR) spectroscopy is an established method for at-line, online, and in-line bioprocess analysis and monitoring, especially in the mid-IR region (400−4000 $cm^{-1}$). Because water, a strong infrared absorber, is the most abundant solvent and maximum interaction lengths are a few tens of micrometers, attenuated total reflection (ATR) configurations are the most commonly used. The light is totally reflected within an ATR element, resulting in an evanescent field that interacts with the sample, with typical penetration depths of approximately 1 to 2 $\mu$m.[1] Multiple reflections lead to enhanced interaction with the sample without having to face the challenges encountered when measuring transmission (clogging, path length changes due to pressure drops, etc.). Multivariate data analysis can be used to extract chemical information from data (i.e., chemometrics); this makes quantification of spectroscopic measurements possible. Lourenço et al.[2] gave a good general overview of optical spectroscopy methods in combination with chemometrics used for bioreactor monitoring, including mid-IR spectroscopy, whereas a mini-review by Landgrebe et al.[3] summarizes recent applications of near- and mid-IR spectroscopy for bioprocess monitoring. A frequently used chemometric method is principal component analysis (PCA). ATR mid-IR spectroscopy in combination with PCA has been, e.g., successfully used for the classification and identification of chemical differences of edible fats and oils,[4] *Robusta* and *Arabica* coffees,[5] and injured and intact *Listeria monocytogenes*.[6]

For various bioprocesses, spectra of media components and excreted secondary metabolites have been recorded at-line,[7−10] online, and in-line. Online bypass systems were successfully

**Received:** November 5, 2014
**Accepted:** January 12, 2015
**Published:** January 12, 2015

  

DOI: 10.1021/ac504126v
*Anal. Chem.* 2015, 87, 2314−2320

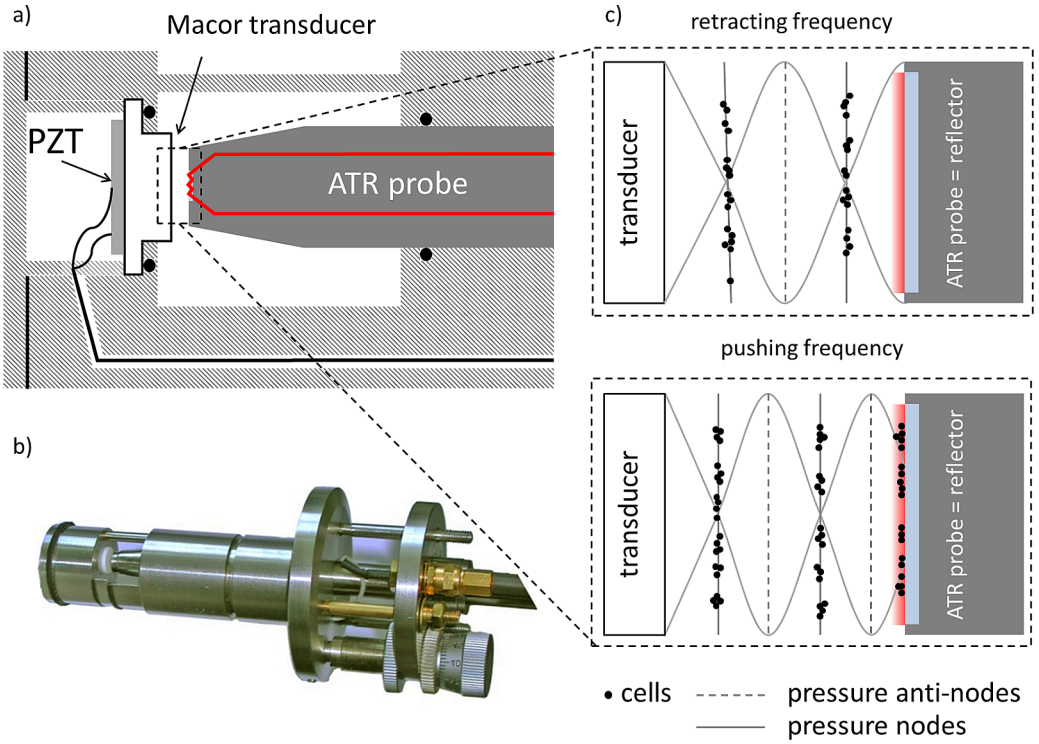


**Figure 1.** Schematic (a) and photograph (b) of the prototype probe: commercial ATR probe and the custom-built ultrasound accessory. (c) The two operating modes. The cells and the evanescent field are magnified by a factor of 10 in comparison to the other dimensions for visibility.

used to monitor media composition and products[11−13] and for pH control[14] in different types of bioprocesses. In-line ATR probes are realized using fiber optics (typically, silver halide) or light conduits and are commercially available. Doak and Phillips reported the first use of a conduit probe to monitor *Escherichia coli* fermentation in 1999;[15] since then, numerous reports of in-line, i.e., in situ (the more commonly used term in bioprocess engineering), monitoring of fermentation have been published.[16−20]

Spectra of microorganisms are acquired at-line or off-line and allow for differentiation between physiological states, reflected by biochemical composition and the quantification of secondary metabolites accumulated inside cells. In most studies, transmission spectra of washed, dried cells were measured, either by FT-IR microspectroscopy[21,22] or with the dedicated microplate reader accessory HTS-XT for high-throughput analysis (Bruker Optics).[23−27] Transmission and ATR FT-IR microspectroscopy were successfully used for the analysis and differentiation of physiological states in the yeast *Saccharomyces cerevisiae*.[28−31] Jarute et al. presented the first online setup for the quantification of poly beta-hydroxybutyic acid (PHB) in *E. coli* using a horizontal ATR in combination with a stopped-flow system.[32] When the flow was on, spectra of the medium were acquired; subsequently, the flow was switched off, and the cells sedimented onto the ATR surface and thus spectra of the cells could be acquired. Biofouling was avoided by chemical cleaning of the ATR as necessary.

**Ultrasound Particle Manipulation.** Ultrasonic standing wave fields, built up between an ultrasound transducer and a reflector, are a contact-free, gentle method for manipulation of small particles in suspension. Particle sizes between one and a few tens of micrometers require ultrasound frequencies between 1 and 10 MHz. The axial acoustic radiation force, i.e., in the direction of sound propagation, acting on the particles depends on particle volume, the ultrasound frequency, the acoustic energy density, i.e., the power that is transmitted into the medium, and the acoustic contrast factor.[33−35] The force results in a pattern of planes that are half of a wavelength apart, into which the particles are driven. These planes are either the pressure nodal planes (i.e., the planes of minimum acoustic pressure) or the pressure antinodal planes of the standing wave field, depending on the acoustic contrast factor between the particles and the carrier medium. This, in turn, depends on the ratio of the sound speeds and mass densities between the particles and the medium; dense particles, like cells, are driven into the pressure nodes of the standing wave field. Ultrasound particle manipulation is not harmful to cells[36,37] and is a state-of-the-art method for perfusion filtering of mammalian cell cultures, where it is used to hold cells against a continuous flow of medium.[38−40]

Ultrasound particle manipulation was used to increase the robustness of online cell spectra acquisition (*S. cerevisiae*) in a setup similar to that of Jarute et al.,[32] by using the radiation force to lift the cells off of the horizontal ATR surface, which acted as ultrasound reflector.[41] Furthermore, the settling speed, and thus the measurement intervals, could be increased by the formation of cell aggregates in the pressure nodal planes, which sedimented faster than single cells once the ultrasound and the flow were switched off. A major drawback of bypass setups are sterility issues. This can be overcome by taking the system in-line.[42] Radel et al. showed in 2010 that the combination of ultrasound particle manipulation and a fiber optic ATR probe made acquisition of mid-IR spectra of PTFE particles in stirred suspensions possible.[43] Here, the ATR element was oriented vertically, and the particles were pushed against it by tuning the ultrasound frequency such that a net acoustic radiation force acted in the direction of the ATR element. In 2013, we showed


DOI: 10.1021/ac504126v
*Anal. Chem.* 2015, 87, 2314−2320

that spectra of *S. cerevisiae* could be acquired with a prototype in-line applicable probe.[44]

This article presents a major step forward in this development: an autoclavable, in-line ultrasound-enhanced fiber optic mid-IR ATR probe constructed according to FDA guidelines and its application during *S. cerevisiae* fermentation in-line in a semi-industrial fermenter. Within fed-batch fermentation, the cells were deliberately nitrogen-limited by the design of the media and therefore started to accumulate storage carbohydrates, i.e., trehalose and glycogen, which was investigated. We recently showed the possibility of off-line quantification of these carbohydrates in whole *S. cerevisiae* by FT-IR microspectroscopy.[31] Here, we investigated the possibility of monitoring these biochemical changes in-line by comparing them to off-line reference spectra and principal component analysis.

## EXPERIMENTAL SECTION

**Ultrasound-Enhanced Fiber Optic ATR FT-IR Probe. Spectrometer and In-Line Probe.** FT-IR spectra were acquired in-line with the process spectrometer ReactIR 15 equipped with an attenuated total reflection DS DiComp (diamond) 9.5 mm probe connected via a 1.5 m AgX (silver halide) fiber (all Mettler Toledo, Greifensee, Switzerland). The spectrometer was equipped with a liquid nitrogen cooled mercury−cadmium−telluride (MCT) detector. Spectra were acquired with resolutions of 4 and 8 $cm^{-1}$, respectively, in the spectral region from 700 to 2800 $cm^{-1}$ as the co-addition of 256 scans. iC IR 4.2 software (Mettler Toledo, Greifensee, Switzerland) was used for acquisition and basic data manipulation such as single-point baseline offset correction (1840 $cm^{-1}$ set to zero). The DS DiComp probe was chosen due to its flat top, which makes it especially suitable as a reflector for the ultrasonic wave.

**Ultrasound Technology: Material and Design Considerations.** The fiber optic probe was equipped with an in-house-designed ultrasound accessory that allowed for manipulation of particles in suspension (Figure 1a,b). The materials were chosen with consideration of FDA regulations, i.e., standard materials used in biotechnology were applied (body, stainless steel material no. 1.4571/DIN X6CrNiMoTi17-12-2; screws, stainless steel A4 (1.4404) (Bossard, Zug, Switzerland); seals and O-rings, ZruElast and ZruElast FPM 75 shore (both Zrunek, Vienna, Austria)). The ultrasound composite transducer consisted of a 10 mm PZT (lead zirconium titante, type PIC 181, PI Ceramics, Lederhose, Germany) disc with wrap-around silver electrodes glued to a Macor cylinder with a one-component epoxy resin (Araldite AV 171, Huntsman Advanced Materials, The Woodlands, TX, USA). The assembled ultrasound-enhanced mid-IR ATR probe complies with the 3D rule to avoid turbulent flow stagnation, i.e., indentations were limited to three times their respective widths, and it is autoclavable in situ (121 °C, 20 min). A modified (limited to 2.5 W max power output) frequency power synthesizer (FPS 2540, SinePhase Instruments, Hinterbrühl, Austria) connected to the PZT was used for ultrasound signal generation and amplification; frequency and power were controlled using a custom LabView script and GUI (National Instruments, Austin, TX, USA). The distance between the ultrasound transducer and ATR probe was adjusted to approximately 1.35 mm.

The working principle is shown in the inset in Figure 1c: At retracting frequency $f_r$, cells are held in the pressure nodal planes away from the evanescent field of the ATR probe, whereas they are pushed against the ATR surface and thus into the evanescent field when the pushing frequency $f_p$ is applied.

**Laboratory FT-IR Spectrometers: Reference Spectra.** Reference spectra of glucose, trehalose, and mannan solutions and glycogen mixed with $H_2O$ were acquired with a Tensor 37 FT-IR spectrometer equipped with a DTGS (deuterated triglycine sulfate) detector using a Platinum diamond ATR (all Bruker Optics, Ettlingen, Germany). Instrument control and spectrum acquisition were performed with OPUS 7 software (Bruker Optics). Spectral resolution was set to 2 $cm^{-1}$, and spectra were recorded as the co-addition of 32 scans.

Sampling, pretreatment of the off-line samples, and acquisition of reference spectra of dried yeast samples drawn during fermentation have been described elsewhere.[31]

***S. cerevisiae* Cultivations.** Fermentation of *S. cerevisiae* (strain CBS8340) was carried out in two different, fully automated and controlled stirred bioreactors: a 10 L glass/steel bioreactor (Chemap, Switzerland) and a 15 L steel bioreactor (Infors, Bottmingen, Switzerland). Both were equipped with 25 mm Ingold ports for coupling with the ultrasound-enhanced mid-IR ATR probe. Media preparation and cultivation conditions are described in detail in the Supporting Information (Experimental, page S2, and Table S1, page S2); the stirring speed was varied (800−1200 rpm), and the $pO_2$ level was always kept above 80% by adjusting the inflow of air. $CO_2$ content of the off-gas was measured using an off-gas analyzer (Bluesens, Snirgelskamp, Germany). Biomass was determined off-line by measuring the optical density at 600 nm with a Genesys 20 visible spectrophotometer (Thermo Scientific, Waltham, MA, USA).

After the batch phase on glucose was completed, the bioprocess was carried on as a C-limited fed-batch with an exponential feed strategy. The feed medium was deficient in a nitrogen source. Under C-limited feeding conditions, no excess carbon source was present in the medium. The nitrogen limitation led to the synthesis and accumulation of storage carbohydrates, i.e., trehalose and glycogen, inside the cells.

**Experimental Procedure for Ultrasound-Enhanced Mid-IR Spectroscopy.** During fermentations, $f_p$ was 2.410 MHz at 1.8−1.9 W true electrical power input (t.e.p.i.), and $f_r$ was 1.870 MHz at 1.6 W t.e.p.i.

**Data Analysis.** Matlab (Mathworks, Natick, MA, USA) and the PLS toolbox (Eigenvector Research, Wenatchee, WA, USA) were used for data manipulation and PCA. For PCA, the spectra were area normalized in the carbohydrate region (938−1186 $cm^{-1}$) prior to calculation of the second derivate (Savitzky-Golay, second order, window width 9 or 11 depending on spectral resolution). Single-analyte spectra were normalized and differentiated using the same settings for comparison.

## RESULTS AND DISCUSSION

**In-Line Procedure.** Spectra were acquired in-line during fermentation, alternating between pushing and retracting frequency every 10 min. Three FT-IR spectra were acquired at each ultrasound frequency; they were subsequently averaged for further data analysis, resulting in a single, average, spectrum for each frequency application. The background was acquired in batch medium with the probe in its final position in the bioreactor after autoclaving. This was used as the background for the absorbance spectra of the medium, i.e., spectra recorded during the application of the retracting frequency. Absorbance


DOI: 10.1021/ac504126v
*Anal. Chem.* 2015, 87, 2314−2320

spectra of the cells were calculated as difference spectra between a spectrum acquired during the application of the pushing frequency and the respective previous media spectrum (Figure 2). This was necessary to compensate for changes in

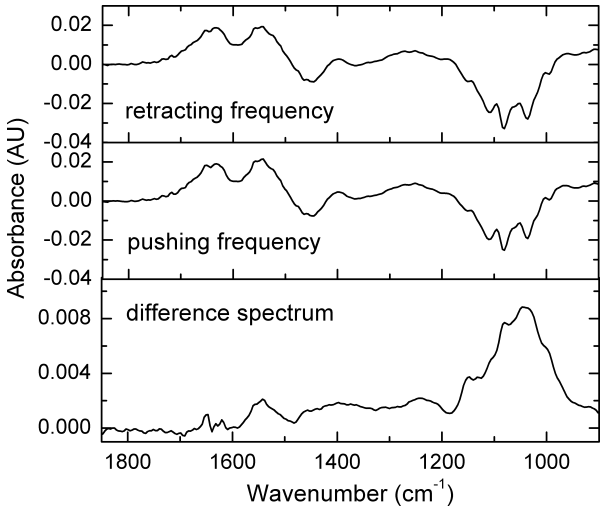


**Figure 2.** In-line spectra acquired during *S. cerevisiae* fermentation when applying retracting frequency (top) or pushing frequency (middle) and their difference spectrum showing typical spectral features of yeast cells.

the medium composition, as there is always medium in the probed volume and analyte concentrations are higher (and vary stronger over the course of the fermentation) in the medium than in the cells themselves. Samples were drawn from the bioreactor at different times for biomass determination and the acquisition of cell reference spectra.

**Optimization of Experimental Conditions.** In total, four fermentations were conducted; the influence of the ultrasound frequency for pushing and retracting, stirring speed, and spectral and temporal resolution were investigated, and the optima were subsequently used. The highest yeast-related absorption values in difference spectra were found using a pushing frequency of 2.410 MHz and a power of 1.8−1.9 W t.e.p.i. ($f_p$). For retracting the particles from the evanescent field of the ATR element, the ultrasound transducer was driven around $f_r$ 1.870 MHz (at 1.6 W t.e.p.i.). Stirring speeds between 600 and 1200 rpm were tested: an increase in stirring speed led to a decrease of absorption values of the recorded spectra due to Stokes drag (data not shown). As a compromise between sufficient stirring and satisfactory signal of the mid-IR spectra of cells, a stirring speed of 800 rpm was identified. Comparison of spectral resolutions of 4 and 8 $cm^{-1}$ showed that the broad absorption bands of *S. cerevisiae* were sufficiently resolved by the latter (data not shown). Temporal resolution was governed by spectrum acquisition time (i.e., 1 min at 8 $cm^{-1}$ resolution and co-addition of 256 scans), sufficient data redundancy (in case of erroneous spectra and to increase the signal-to-noise ratio), and maximum handleable file size. Spectra were acquired every 2 min; thus, as mentioned before, three spectra were available for averaging during alternating application of the ultrasound frequencies for 10 min each. These parameters were determined during the first fermentation and were subsequently used. The spectra recorded during the four fermentations showed similar trends, and an exemplary one will be presented here.

**Influence of Growth Conditions on Yeast Cells.** In order to study changes on the (bio)chemical composition of the cells, the fermentation was carried out in two parts: a batch phase, with an excess of glucose (C-source) and ammonium (N-source), and subsequently a C-limited fed-batch phase during which no additional N-source was fed and trehalose and glycogen were accumulated inside the cells.

**Batch Phase.** At the beginning of the batch phase, glucose was present in excess in the medium, leading to the production of ethanol as a main metabolite in addition to biomass (Crabtree effect, overflow metabolism). The cells exhibited characteristic diauxic growth: first, glucose was metabolized to ethanol in parallel with biomass formation (0−12 h) and then, after a short lag phase, the extracellular ethanol was metabolized as a carbon source (12−20 h). This was reflected by the $CO_2$ off-gas profile and the FT-IR spectra of the medium (Figure 3).

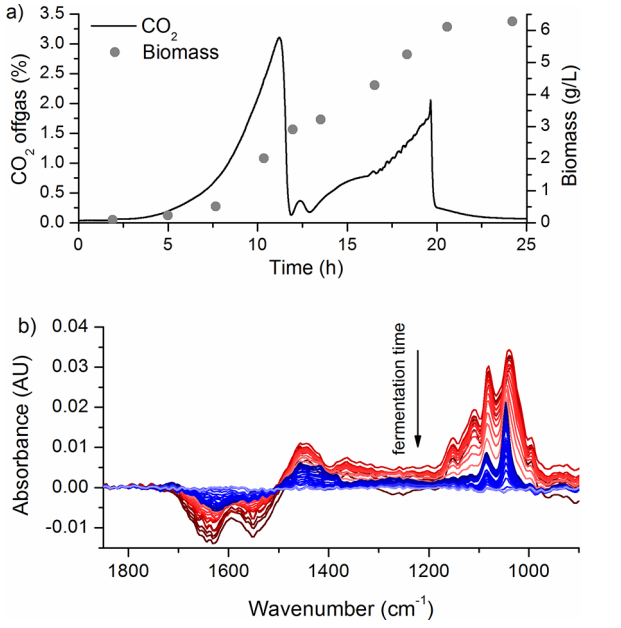


**Figure 3.** (a) $CO_2$ off-gas and biomass over the course of the batch phase. (b) ATR FT-IR spectra of the medium (i.e., retracting frequency applied) over the course of the batch phase.

Characteristic spectral features of glucose were predominant at first (Figure 3b, dark red spectra, bands at 1150, 1110, 1080, and 1037 $cm^{-1}$) followed by a superposition of glucose and ethanol (light red spectra). Once the glucose was depleted, ethanol dominated the FT-IR spectra, with its characteristic bands at 1045 and 1080 $cm^{-1}$ (blue spectra), which gradually decreased until the end of the batch phase (light blue spectrum).

During batch phase, yeast cell composition did not change; only biomass growth occurred, which was reflected by an increase in absorbance over time, whereas spectral features remained similar (see Supporting Information Figure S1).

**Fed-Batch Phase.** The spectra of dried *S. cerevisiae* fed-batch samples acquired off-line (Figure 4a) show spectral features typical for the constituents of biological cells (from refs 45 and 46): The C═O stretching of ester groups in lipids leads to an absorption around 1730 $cm^{-1}$. Proteins lead to absorptions around 1655 $cm^{-1}$ (amide I band, mainly from C═O stretching and, to a lesser extent, N−H bend and C−N stretch), around 1550 $cm^{-1}$ (amide II band, N−H bend, and



DOI: 10.1021/ac504126v
*Anal. Chem.* 2015, 87, 2314−2320

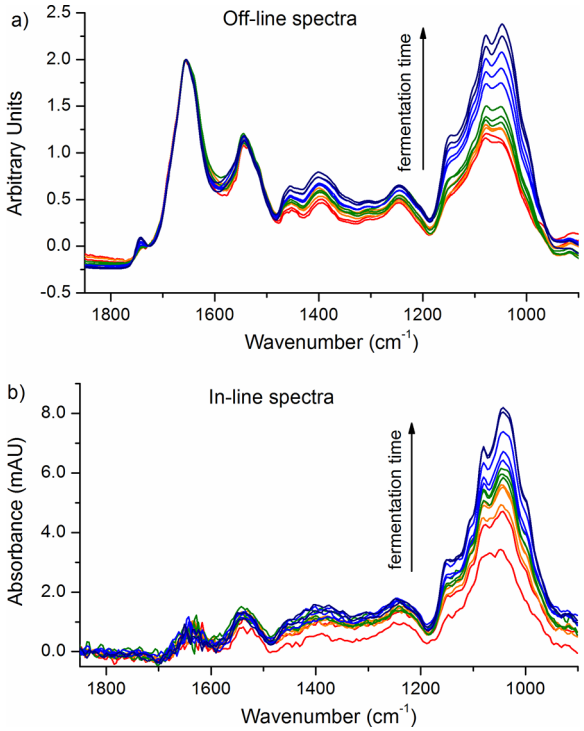


**Figure 4.** (a) Spectra of dried *S. cerevisiae* acquired off-line using a laboratory FT-IR microscope (normalized to amide I band). (b) Spectra of *S. cerevisiae* acquired in-line using the ultrasound-enhanced mid-IR ATR probe at the times when samples for off-line analysis were drawn.

C−N stretch), and around 1300 $cm^{-1}$ (amide III band, complex combination of different vibrations). In the region between 1450 and 1200 $cm^{-1}$, numerous C−H and O−H deformation vibrations contribute to the spectrum (lipids, carbohydrates). Antisymmetric $PO_2^-$ stretching vibrations of DNA, RNA, and phospholipids lead to absorptions around 1240 $cm^{-1}$. The region between 950 and 1200 $cm^{-1}$ (hereafter, carbohydrate region) is dominated by C−O stretching originating from carbohydrates, with contributions around 1100 $cm^{-1}$ from symmetric $PO_2^-$ stretching (again, DNA, RNA, and phosopholipids).

The changes in carbohydrate content induced by N-limited growth are reflected by changes in the shape of the spectra acquired off-line (Figure 4a, normalized to the amide I band). The relative carbohydrate content increases with fermentation time, and the shape of the carbohydrate region changes as trehalose and glycogen are formed in the cells. The carbohydrate bands of the difference spectra of the cells acquired in-line at the time points of sampling (Figure 4b, offset baseline corrected) are in good agreement with the off-line spectra (Figure 4a). Differences can be attributed to matrix influence, band shifts due to acquisition in ATR mode, and the lower signal-to-noise ratio for in-line spectra.

A major difference between the off- and in-line measurements was observed in the amide I and amide II regions: here, $H_2O$ absorbs strongly (H−O−H bending at approximately 1640 $cm^{-1}$) and therefore the intensity reaching the detector is low, leading to a high noise level. The protein bands (amide I and II) are only weakly visible in the in-line spectra, most likely because the $H_2O$ present when the $f_r$ spectrum is acquired is simply replaced by the protein present in *S. cerevisiae* when $f_p$ is applied, leading to approximately the same absorption. Furthermore, when $f_p$ is applied, $H_2O$ is, for the most part but never completely, replaced by yeast cells (even assuming close packing of equal spheres, approximately 26% of the space would still be occupied by $H_2O$).

Since changes associated with switching to nitrogen-limited growth are mainly visible in the carbohydrate region of the FT-IR spectra, further analysis was focused on this region. The main carbohydrates of yeast were studied: mannan, a cell wall polysaccharide composed of mannose units, and intracellular carbohydrates trehalose, a disaccharide of glucose, glycogen, a polysaccharide of glucose, and glucose. ATR FT-IR reference spectra of the major carbohydrates (area normalized as described in the Experimental Section) present in yeast cells are shown in Figure 5a. At 994 $cm^{-1}$, trehalose, one of the

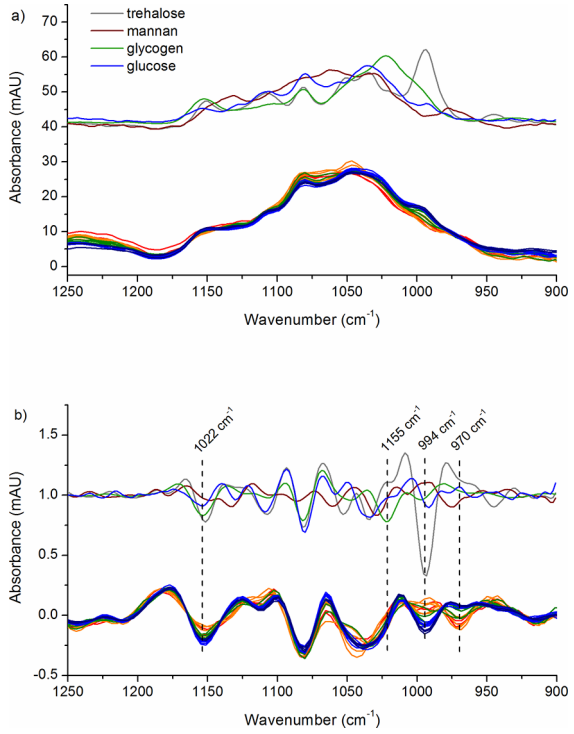


**Figure 5.** (a) Spectra of major carbohydrates present in yeast cells (off-line ATR, in solution) and spectra of yeast cells acquired in-line over the course of the fermentation. (b) Second-derivative spectra of major carbohydrates present in yeast cells and of yeast cells acquired over the course of the fermentation, respectively. In both graphs, carbohydrate spectra are offset for better visibility.

storage carbohydrates accumulated during N-limited growth, has an intense and specific absorption. In the spectral region between 1025 and 1175 $cm^{-1}$, trehalose and glucose show bands at similar positions; their relative intensities are, however, different. Glucose absorbs strongest at 1035 $cm^{-1}$, whereas the relative absorption maximum of trehalose in this region is shifted toward slightly higher wavenumbers and is lower in intensity. At around 1155 $cm^{-1}$, trehalose and glycogen have a common absorption band. Glycogen absorbs broadly between 970 and 1170 $cm^{-1}$, with a distinct maximum at 1022 $cm^{-1}$ and smaller maxima at 1080 and 1152 $cm^{-1}$. Mannan has a broad absorption band between 1000 and 1150 $cm^{-1}$, with a distinct maximum at 1060 $cm^{-1}$. The exact positions of absorption maxima are even clearer when looking at second derivatives of the spectra: maxima in the spectra are minima here (Figure 5b, top).


DOI: 10.1021/ac504126v
*Anal. Chem.* 2015, 87, 2314−2320

In the yeast, changes in the carbohydrate composition can be observed by spectra acquired in-line as difference spectra over the course of the N-limited fed-batch fermentation (Figure 5a, bottom). The shape of the carbohydrate band changed with fermentation time, most notably between 1050 and 950 $cm^{-1}$. The blue spectra, which were acquired toward the end of the fermentation, show higher absorption around 990 $cm^{-1}$, correlating well with the absorption spectra of trehalose. This becomes even clearer when investigating second-derivate spectra: The decrease around 994 $cm^{-1}$ and the increase around 970 $cm^{-1}$ in the spectra acquired toward the end of the fermentation (blue) correlate well with the trehalose second-derivative spectrum (gray). Between 1030 and 1000 $cm^{-1}$, the slope of the second-derivative yeast spectra steepens with fermentation time. The minimum at ~1150 $cm^{-1}$, which further decreases with fermentation time, correlates with an increase in both glycogen and trehalose. Since this minimum is less pronounced for trehalose compared to the one at 994 $cm^{-1}$, it can be concluded that glycogen mainly contributes to this change.

**PCA.** We have recently shown that quantitative determination of carbohydrates is possible from off-line yeast spectra;[31] from the in-line difference spectra, only qualitative information on the changes in carbohydrate composition could be observed. Normalization of the spectra proved to be difficult because changes in biomass and in the carbohydrate content occurred simultaneously, and this correlation could not be broken. To evaluate if the trends observed in the in-line difference spectra are statistically detectable and related to carbohydrate features, PCA was performed on the second-derivative spectra.

Individual PCA of the four fermentations resulted in very similar principal component 1 (PC1), which explained between 53 and 73% of the variation in the respective fermentation spectra. A PCA of the combined spectra from all four fermentations again resulted in a PC1 with very similar features; however, only 40% of the variance was explained. This can be attributed to interfermentation variations leading a smaller contribution from changes induced by N-limited growth. To concentrate on the biochemical changes inside the cells, the following discussion is based on the PCA of a single fermentation.

The loading vector of PC1 and the second-derivative spectra of trehalose, glycogen, glucose, and mannan show similar features (Figure 6). Spectral region A (1020−970 $cm^{-1}$) of PC1 correlates with trehalose: the minimum is around 995 $cm^{-1}$ for both, followed by a maximum at 980 $cm^{-1}$ and a shoulder around 960 $cm^{-1}$. This region also varies the most between spectra, reflected by the highest values of the first loading vector. The plateau at 1035 $cm^{-1}$ followed by a minimum around 1025 $cm^{-1}$ in PC1 correlates with glycogen, superimposed with trehalose and glucose (thus, the shift of the minimum toward higher wavenumbers). In spectral region B (1050 to 1103 $cm^{-1}$), trehalose, glycogen, glucose, and PC1 show very similar features, and a clear attribution cannot be made. Around 1155 $cm^{-1}$ (spectral region C), the minimum in PC1 corresponds to a superposition of the minima of both trehalose and glycogen.

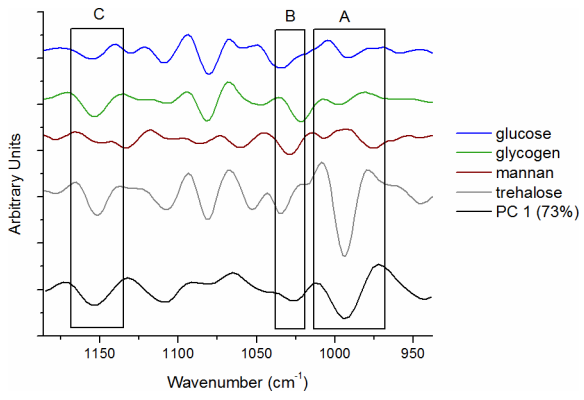


**Figure 6.** Second-derivative spectra of trehalose, glycogen, glucose, and mannan and PC1 of spectra acquired during N-limited growth.

## CONCLUSIONS AND OUTLOOK

The presented method allows for the selective acquisition of mid-IR spectra of either dissolved analytes (media components) or suspended particles (cells). This is, to the best of our knowledge, the first report on the acquisition of mid-IR spectra of microorganisms (*S. cerevisiae*) inside a semi-industrial bioreactor during fermentation without the necessity of drawing a sample. The cell spectra acquired in-line are in good agreement with spectra of dried cell samples that were recorded off-line. Trends in the changes of the biochemical composition of the cells during N-limited fed-batch fermentation were visible, showing the potential of ultrasound-enhanced ATR mid-IR spectroscopy to be used as a PAT (process analytical technology) probe to detect the cells' physiological response to nutritional limitations. Quantitative analysis proved to be difficult, as the number of cells present in the evanescent field is hard to estimate and the amide I band, which could be used for normalization off-line, was not accessible in-line. Furthermore, the signal-to-noise ratio of the difference spectra still needs to be improved to make quantitative analysis by, e.g., partial least-squares regression possible. More insight into the spatial distribution of the cells in the evanescent field could potentially be gained using the gel method proposed by Gherardini et al.;[47] with a better understanding of the number of cells held in the evanescent field at a given time under different conditions, the before-mentioned challenges will be addressed in a follow-up project.

The described novel method is generic and suitable for (ideally spherical) cells within a size range of 1 to approximately 40 $\mu$m, as is often employed in white and red biotechnology and biorefinery. It delivers real-time information on the chemical composition of cells in situ, thus aiding the optimization of process conditions and media composition. Moreover, physiological responses of cells can be investigated, helping to obtain a basic understanding of cell physiology/metabolism. In industrial fermentation, the method could serve as a quality control tool: here, complex media are often employed, for which exact determination of nutrient concentrations would usually require extensive and laborious chemical analyses or is not possible at all. By measuring the cell's biochemical composition, potential limitations could be detected, and appropriate measures to ensure the desired quality could be taken early in the process.

Apart from bioprocesses, the presented method can, for example, be applied to gain insight into crystallization processes.



DOI: 10.1021/ac504126v
*Anal. Chem.* 2015, 87, 2314−2320

## ■ ASSOCIATED CONTENT

### Supporting Information

Experimental details on media preparation and cultivation conditions. Table S1: Overview of the setup and conditions of the fed-batch fermentations. Figure S1: Spectra of *S. cerevisiae* acquired in-line during batch phase fermentation. This material is available free of charge via the Internet at http://pubs.acs.org.

## ■ AUTHOR INFORMATION


### Corresponding Author

*E-mail: bernhard.lendl@tuwien.ac.at.

### Present Addresses

[§](M.B.) Research Center for Non Destructive Testing GmbH, Altenbergerstraße 69, 4040 Linz, Austria.

[∥](B.Lo.) Division of Life Sciences—Industrial Biotechnology, Department of Chemical and Biological Engineering, Chalmers University of Technology, Kemivägen 10, 412 96 Gothenburg, Sweden.


### Notes

The authors declare no competing financial interest.

## ■ ACKNOWLEDGMENTS


The authors express their gratitude to Lukas Strobl for realization of the Labview control of the ultrasound frequency generator and Gerhard Fritsch for assistance in the assembly of the prototype probe and with preliminary experiments. Partial financial support provided by the Austrian Research Promotion Agency (FFG) under the scope of the COMET program within the research network "Process Analytical Chemistry (PAC)" (contract no. 825340) (C.K. and M.B.) and the Austrian Science Fund FWF (project no. P24154-N17) (C.K. and S.R.) is gratefully acknowledged. C.K. gratefully acknowledges partial financial support by the AB-Tec graduate school (TU Wien). European Social Fund from European Union and Junta de Comunidades de Castilla-La Mancha are gratefully acknowledged for supporting given through a Postdoctoral research contract for M.R.P.


## ■ REFERENCES


(1) Griffiths, P. R.; de Haseth, J. A. *Fourier Transform Infrared Spectrometry*, 2nd ed.; Wiley-Interscience: Hoboken, NJ, 2007; pp 321−348.

(2) Lourenço, N. D.; Lopes, J. A.; Almeida, C. F.; Sarraguça, M. C.; Pinheiro, H. M. *Anal. Bioanal. Chem.* **2012**, *404*, 1211−1237.

(3) Landgrebe, D.; Haake, C.; Höpfner, T.; Beutel, S.; Hitzmann, B.; Scheper, T.; Rhiel, M.; Reardon, K. F. *Appl. Microbiol. Biotechnol.* **2010**, *88*, 11−22.

(4) Dupuy, N.; Duponchel, L.; Huvenne, J. P.; Sombret, B.; Legrand, P. *Food Chem.* **1996**, *51*, 245−251.

(5) Briandet, R.; Kemsley, E. K.; Wilson, R. H. *J. Agric. Food Chem.* **1996**, *44*, 170−174.

(6) Lin, M.; Al-Holy, M.; Al-Qadiri, H.; Kang, D.-H.; Cavinato, A. G.; Huang, Y.; Rasco, B. A. *J. Agric. Food Chem.* **2004**, *52*, 5769−5772.

(7) Sivakesava, S.; Irudayaraj, J.; Ali, D. *Process Biochem.* **2001**, *37*, 371−378.

(8) Franco, V. G.; Perín, J. C.; Mantovani, V. E.; Goicoechea, H. C. *Talanta* **2006**, *68*, 1005−1012.

(9) Roychoudhury, P.; Harvey, L. M.; McNeil, B. *Anal. Chim. Acta* **2006**, *561*, 218−224.

(10) Roychoudhury, P.; McNeil, B.; Harvey, L. M. *Anal. Chim. Acta* **2007**, *585*, 246−252.

(11) Kansiz, M.; Gapes, J. R.; McNaughton, D.; Lendl, B.; Schuster, K. C. *Anal. Chim. Acta* **2001**, *438*, 175−186.

(12) Mazarevica, G.; Diewok, J.; Baena, J. R.; Rosenberg, E.; Lendl, B. *Appl. Spectrosc.* **2004**, *58*, 804−810.

(13) Schenk, J.; Marison, I. W.; von Stockar, U. *J. Biotechnol.* **2007**, *128*, 344−353.

(14) Schenk, J.; Marison, I. W.; von Stockar, U. *Biotechnol. Bioeng.* **2008**, *100*, 82−93.

(15) Doak, D. L.; Phillips, J. A. *Biotechnol. Prog.* **1999**, *15*, 529−539.

(16) Pollard, D.; Buccino, R.; Connors, N.; Kirschner, T.; Olewinski, R.; Saini, K.; Salmon, P. *Bioprocess Biosyst. Eng.* **2001**, *24*, 13−24.

(17) Kornmann, H.; Rhiel, M.; Cannizzaro, C.; Marison, I.; von Stockar, U. *Biotechnol. Bioeng.* **2003**, *82*, 702−709.

(18) Kornmann, H.; Valentinotti, S.; Duboc, P.; Marison, I.; von Stockar, U. *J. Biotechnol.* **2004**, *113*, 231−245.

(19) Dahlbacka, J.; Weegar, J.; von Weymarn, N.; Fagervik, K. *Biotechnol. Lett.* **2012**, *34*, 1009−1017.

(20) Koch, C.; Posch, A. E.; Goicoechea, H. C.; Herwig, C.; Lendl, B. *Anal. Chim. Acta* **2014**, *807*, 103−110.

(21) Kansiz, M.; Billman-Jacobe, H.; McNaughton, D. *Appl. Environ. Microbiol.* **2000**, *66*, 3415−3420.

(22) Stehfest, K.; Toepel, J.; Wilhelm, C. *Plant Physiol. Biochem.* **2005**, *43*, 717−726.

(23) Dean, A. P.; Sigee, D. C.; Estrada, B.; Pittman, J. K. *Bioresour. Technol.* **2010**, *101*, 4499−4507.

(24) Wagner, H.; Liu, Z.; Langner, U.; Stehfest, K.; Wilhelm, C. *J. Biophotonics* **2010**, *3*, 557−566.

(25) Winder, C. L.; Cornmell, R.; Schuler, S.; Jarvis, R. M.; Stephens, G. M.; Goodacre, R. *Anal. Bioanal. Chem.* **2011**, *399*, 387−401.

(26) Scholz, T.; Lopes, V. V.; Calado, C. R. C. *Biotechnol. Bioeng.* **2012**, *109*, 2279−2285.

(27) Corte, L.; Rellini, P.; Roscini, L.; Fatichenti, F.; Cardinali, G. *Anal. Chim. Acta* **2010**, *659*, 258−265.

(28) Burattini, E.; Cavagna, M.; Dell'Anna, R.; Malvezzi Campeggi, F.; Monti, F.; Rossi, F.; Torriani, S. *Vib. Spectrosc.* **2008**, *47*, 139−147.

(29) Cavagna, M.; Dell'Anna, R.; Monti, F.; Rossi, F.; Torriani, S. *J. Agric. Food Chem.* **2010**, *58*, 39−45.

(30) Kuligowski, J.; Quintás, G.; Herwig, C.; Lendl, B. *Talanta* **2012**, *99*, 566−573.

(31) Plata, M. R.; Koch, C.; Wechselberger, P.; Herwig, C.; Lendl, B. *Anal. Bioanal. Chem.* **2013**, *405*, 8241−8250.

(32) Jarute, G.; Kainz, A.; Schroll, G.; Baena, J. R.; Lendl, B. *Anal. Chem.* **2004**, *76*, 6353−6358.

(33) King, L. V. *Proc. R. Soc. London, Ser. A* **1934**, *147*, 212−240.

(34) Yosioka, K.; Kawasima, Y. *Acustica* **1955**, *5*, 167−173.

(35) Gor'kov, L. P. *Phys.−Dokl.* **1962**, *6*, 773−775.

(36) Radel, S.; McLoughlin, A. J.; Gherardini, L.; Doblhoff-Dier, O.; Benes, E. *Ultrasonics* **2000**, *38*, 633−637.

(37) Wiklund, M. *Lab Chip* **2012**, *12*, 2018−2028.

(38) Trampler, F.; Sonderhoff, S. A.; Pui, P. W. S.; Kilburn, D. G.; Piret, J. M. *Nat. Biotechnol.* **1994**, *12*, 281−284.

(39) Gorenflo, V. M.; Smith, L.; Dedinsky, B.; Persson, B.; Piret, J. M. *Biotechnol. Bioeng.* **2002**, *80*, 438−444.

(40) Gorenflo, V. M.; Ritter, J. B.; Aeschliman, D. S.; Drouin, H.; Bowen, B. D.; Piret, J. M. *Biotechnol. Bioeng.* **2005**, *90*, 746−753.

(41) Radel, S.; Schnöller, J.; Gröschl, M.; Benes, E.; Lendl, B. *IEEE Sens. J.* **2010**, *10*, 1615−1622.

(42) Lendl, B.; Radel, S.; Brandstetter, M. Device for FTIR Absorption Spectroscopy. PCT/AT2010/000006, 2010.

(43) Radel, S.; Brandstetter, M.; Lendl, B. *Ultrasonics* **2010**, *50*, 240−246.

(44) Koch, C.; Brandstetter, M.; Lendl, B.; Radel, S. *Ultrasound Med. Biol.* **2013**, *39*, 1094−1101.

(45) Socrates, G. *Infrared and Raman Characteristic Group Frequencies: Tables and Charts*, 3rd ed.; Wiley & Sons Ltd: New York, 2001.

(46) Naumann, D.; Helm, D.; Labischinski, H. *Nature* **1991**, *351*, 81−82.

(47) Gherardini, L.; Radel, S.; Sielemann, S.; Doblhoff-Dier, O.; Gröschl, M.; Benes, E.; McLoughlin, A. *Bioseparation* **2001**, *10*, 153−162.




DOI: 10.1021/ac504126v
*Anal. Chem.* 2015, 87, 2314−2320